

3D Collision-Force-Map for Safe Human-Robot Collaboration

Petr Svarny, Jakub Rozlivek, Lukas Rustler, and Matej Hoffmann

Abstract— Collaborative robots, i.e. robots designed for direct interaction with a human, present a promising step in robotic manufacturing. However, their performance is limited by the safety demands of standards. In this article, we measure the forces exerted by two robot arms (UR10e and Kuka LBR iiwa) on an impact measuring device in different positions in the robot workspace and with various velocities. Based on these measurements, we investigate the Power and Force Limiting regime presented in ISO/TS 15066. Impact forces are in practice hard to calculate analytically as many properties of the robots are not available (e.g., proprietary control algorithms). This motivates the use of simple, yet reasonably accurate, approximations. Our results show that height of the impact location is also an important factor and that an accurate model of the robot can be created from a limited number of impact samples. Previous work predicted impact forces based on other factors (distance, velocity, weight), yet these predictions are less accurate. This would allow a fast estimation of the impact forces in the robot’s workspace and thus make it easier to design a safe human-robot collaboration setup.

I. INTRODUCTION

While *physical Human-Robot Interaction* (pHRI) or *Human-Robot Collaboration* (HRC) saw significant progress, the performance of collaborative robots, i.e. robots designed for direct interaction with humans [1], is bounded by strict demands for safety.¹ Various safety standards, especially ISO 10218 [3] and ISO/TS 15066 [4] (TS 15066 for short), formulate these safety demands. These standards currently list four modes of collaboration. While all HRC is ‘continuous, purposeful interaction associated with potential or accidental physical events’ [5], only the Power and Force Limiting (PFL) mode permits contact between the robot and the human when the robot is still autonomously moving. The mode allows these physical contacts under the condition that the impact force does not exceed the limits given in TS 15066. The technical specification lists various passive or active measures that limit the exerted forces (e.g., increase the contact area, use of sensing to anticipate contacts).

Nevertheless, the suggested force thresholds in the PFL mode enforce low operational velocities for many collaborative applications, especially if there is a risk of clamping (see for example [6] or [7]). These limits motivate the current investigations of the PFL mode that try to overcome its limitations. These investigations can be divided into three perspectives: what PFL deployment maximises performance,

Department of Cybernetics, Faculty of Electrical Engineering, Czech Technical University in Prague, corresponding author: petr.svarny@fel.cvut.cz. The authors would like to thank Minh Thao Nguyenova and Martin Sramek for their valuable suggestions and feedback.

¹Robots can be designed for collaborative operations, but safety can be evaluated only on applications [2].

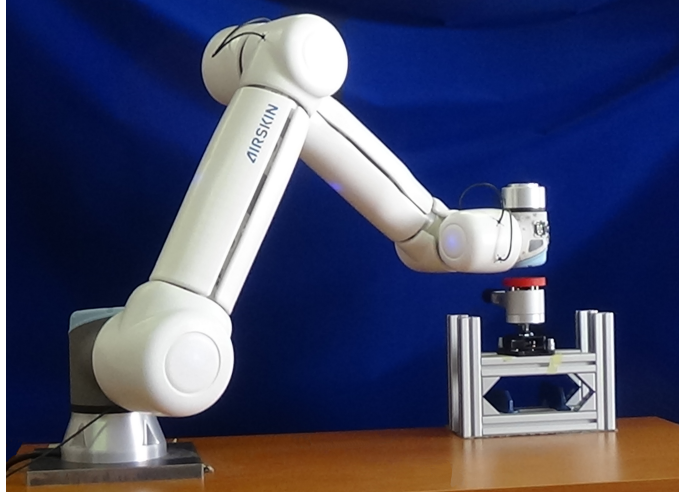


Fig. 1: UR10e with Airskin and measuring device.

what are the proper force limits for safe human-robot collisions, and what is a suitable impact forces model.

The performance of PFL can be improved, when it is combined with the so-called Speed and Separation Monitoring collaboration mode. Already a simple combination [8] improves the overall performance of the system. An even greater performance improvement can be achieved by the use of optimal velocity scaling [7], velocity scaling based on an impact force model [9], the use of control barrier functions [10], or by predicting the exerted force based on the motor currents [11].

While the original TS 15066 presented force limits based on pain thresholds from studies as [12], it also suggested that future studies are necessary to establish the correct threshold values for collaborative robots. However, the study that continues this investigation of pain thresholds [13] finds pain thresholds that are not only lower than those in TS 15066 but show a high variance in between subjects. This finding supports the claim of Mansfeld et al. [6] that “the thresholds [in TS 15066] were not derived from an experiment which aims at finding data-driven relation between collision input parameters and human injury” but that pain thresholds are a very unreliable measure. The proposed human injury thresholds in [6] are more permissive than TS 15066. Nevertheless, the level of acceptable injury needs to be specified. A study of collision effects [14] on a pigskin sample investigates the relevant impact force threshold that would lead to minor injuries and suggests a more restrictive threshold. It proposes a single threshold of 100 N (as opposed to the range 65–210 N based on the properties of different body regions from TS

A detailed treatment of impact force modelling and the safety aspects of human-robot collisions is presented in [15], [16]. The already mentioned [9] models various impactor shapes, but does not draw conclusions with regards to the TS 15066 model as opposed to [6] that explicitly calls out the TS 15066 model as overly simple. Kovincic et al [17][18] suggest using collected impact data to model the impact forces using machine learning approaches because robot reaction mechanisms play a significant role in the resulting forces and are “not known or can not be identified” [17]. The work in [19] is the most relevant to our approach as it introduces a 2D Collision-Force-Map (CFM) and models the impact forces of UR10 and UR10e robots in a pick and place task with a second degree polynomial and uses it for model-based control of the end-effector velocity.

Our work fits into the last category—impact force modelling. We enhance the model from [19] to a 3D Collision-Force-Map (3D CFM) and we collect data to verify how our model fits real data. The suggested model allows to model the impact forces of a robot without access to its intrinsic properties or detailed model. Our method is more precise and less time-consuming than earlier presented methods in the category.

Contributions

Therefore, based on the research of the state of the art, the contributions of this paper are:

- Extension of the previously published model of the impact forces based on the position of the contact by adding the height parameter.
- Presentation of a time-effective data collection method for impact force modelling.
- Comparison of three models for impact forces (the PFL model, the CFM model, and our 3D CFM model).
- Experimental verification of impact forces exerted by two different collaborative robots.

II. MATERIALS AND METHODS

Our goal is to measure impact forces at various locations of the robot workspace using two different standard collaborative robots, UR10e (UR) and Kuka LBR iiwa 7R800 (Kuka), and compare the results to various models of impact forces. In the following sections, we will introduce the data collection method, the setup, the models, and the robots that were used.

A. Data collection method

Schlotzhauer et al. [19] show that the impact force is the same on concentric circles. Based on this assumption it is possible to estimate the 3D workspace by measuring only in two dimensions (ρ , z coordinates in a cylindrical coordinate system, we follow the notation from [19] and use d as distance and h as height, see Fig. 3). However, it is necessary to use the velocity as the third dimension because the impact force depends on it as well. Hundreds of contacts should be done to sample densely the 3D grid

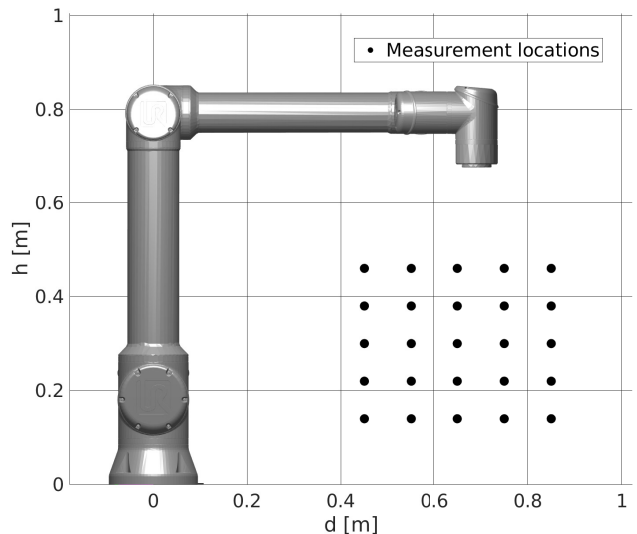


Fig. 2: UR grid of measurement points.

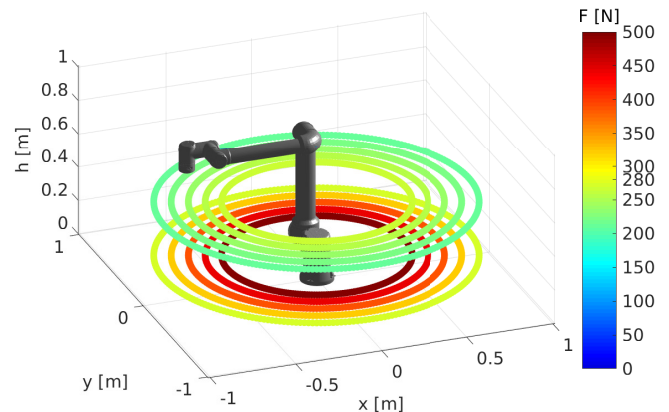


Fig. 3: UR concentric impact force circles at various heights.

and interpolate data precisely which is time-consuming. For example, for CFP more than 400 measurements—5 velocities and 81 d values—(each repeated 3 times) were done at the same height in [19].

We suggest collecting the training data only for all the combinations of the smallest, middle and the largest values of d , h , and speed. This means to perform only 27 measurements (81 if each one is repeated 3 times).

The studied models will be evaluated on their prediction error with the goal to minimise especially underestimation of the impact forces to assure that the predictions are safe.

B. Experiment setup

The experiments were comprised of a series of impacts onto specified positions. These positions were defined to investigate various configurations of the robot in its workspace and we collected a set to train our model and a set to test its predictions. We investigated only linear movements as they lead to the highest impact forces.

We collect data in the workspace of the respective robots at

various heights. For the UR robot, the d range was from 0.45 m to 0.85 m with 0.1 cm increments and with five different heights from the level of the robot's base starting at 0.14 m with 0.08 m increments. Also, additional positions were used to verify the force is the same on concentric circles as mentioned in [19]. Illustration of the measurement setup is in Fig. 2 and the concentric circles are visible in Fig. 3.

The Kuka robot has a different reach. Therefore we sampled the workspace at the following positions: d from 0.56 m to 0.86 m with an increment of 0.075 m and again in five heights corresponding to heights used with UR robot. The increment between positions was shortened to ensure measurements on the same number of positions for both robots. So similarly to the UR robot, we get five circles with radius d from 0.56 m to 0.86 m.

At a given position, we performed measurements with five different speeds—0.20, 0.25, 0.30, 0.35, and 0.40 m/s. The lowest two speeds match those used also in [19]. However, we used higher speeds in order to map the limits of collaborative applications. All of the measurements were repeated three times (unless otherwise stated, see Kuka with 10 Nm in Sec. III-C). All measurements above the devices recommended limit (500 N) were discarded.

C. Robots

Both robots were controlled using their standard control interfaces while experimental data were collected. For clarity we also we specify the safety settings used for the experiment as they influence the resulting impact forces.

We controlled the UR10e via UR script to use the linear motion therein. We collected the velocity data using the Modbus interface and other variables (joint values etc.) from ROS nodes. Our UR is equipped with the protective skin Airskin that adds extra weight (1.8 kg) to the robot, see Fig. 1. The worst-case collection frequency for the robot speed was 800 Hz and 500 Hz for other variables. The second most restrictive safety setting was used, which restricts the robot mainly in force and speed but allows for sufficient acceleration and deceleration with respect to our velocities².

A Java application was written in Kuka Sunrise to control the Kuka robot and a separate application to collect the data from the robot with a frequency of 1000 Hz. The Kuka is equipped with a joint-torque sensor in each of its joints and the safety setting restricts the maximal external torque at any joint. Two different settings were used to verify if these settings are an important factor too—10 and 30 Nm.

Due to various technical limitations (e.g., sensitive equipment on the Kuka's end-effector), we measured collisions not with the end-effector but with the last joint's surface.

D. Measuring device

The impacts were measured using the *CBSF-75-Basic* measuring device that is meant to be used during the validation of collaborative applications of robots (see [20]

²Allowed power: 200 W, Momentum: 10 kg m/s, Stopping time: 300 ms, Stopping distance: 300 mm, Tool speed: 750 mm/s, Tool force: 120 N, Elbow speed: 750 mm/s, Elbow force: 120N.

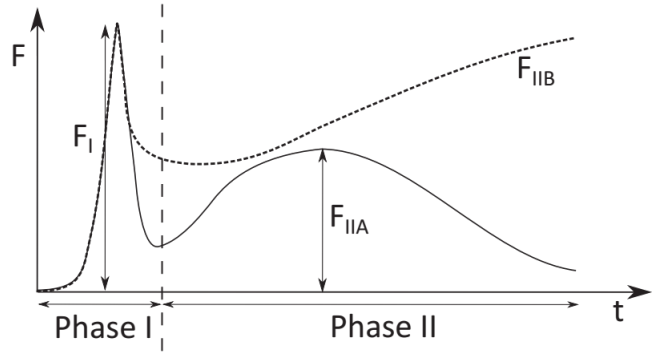


Fig. 4: Collision phases, taken from [15].

referenced also in the TS 15066). It allows the measuring of transient and quasi-static forces of up to 500 N.

In accordance with TS 15066, appropriate K1 damping materials are added to the device in order to simulate the properties of the human body region. Namely, in the case of the Basic 75 N/m device and the damping material with the hardness Sh 70, the measurement mimics impacts on the back of the non-dominant hand.

E. Power and Force Limiting

The PFL regime described in TS 15066 allows us to calculate the maximal permissible velocity for the robot based on the maximum force allowed for a given body area. The permissible force is also determined based on the type of impact. A human-robot collision can be decomposed into two phases (see [15] for details). An initial dynamic impact (part of transient contact in the TS 15066) in Phase I is followed by the Phase II force profile that depends on the clamping nature of the incident (see Fig. 4). If there is no clamping, the contact can resolve into active quasi-static pushing where the force will in general diminish (transient contact in TS 15066). The other case is a clamping scenario (called quasi-static contact by TS 15066) where the force is limited by the maximum motor torques and the robot reaction behavior.

The equation A.6 from TS 15066 relating velocity and impact force is:

$$v \leq \frac{F_{max}}{\sqrt{k}} \sqrt{m_R^{-1} + m_H^{-1}}, \quad (1)$$

where m_R is the effective robot mass, m_H is the human body part mass, k spring constant for the human part body and F_{max} is the maximum impact force permitted for the given body region. As pointed out also by [6], the collision model used in the TS 15066 is a simple spring model.

As mentioned, the risks of HRC cannot be evaluated solely based on the robot. It is necessary to take into account the application as a whole. In our case, we assume a pick and place scenario with a risk of quasi-static contact as in [19]. The contact would occur while the robot is descending towards the table and the human operator is also manipulating the object. In the case of an actual application,

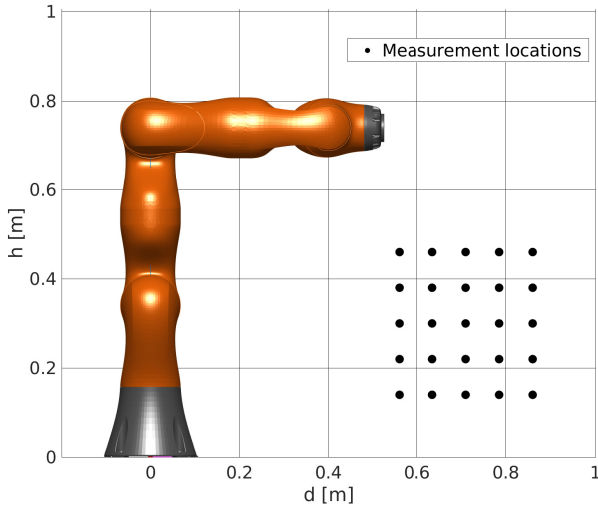


Fig. 5: Kuka grid of measurement points

a detailed risk analysis according to [21] must be performed and the potential clamping spaces identified.

If we investigate a quasi-static contact, even without clamping, we can approximate the m_h as infinite (as in [7]). This approximation allows us also to simplify the situation by investigating the relative velocity as simply the robot velocity with the human hand being still. The other variables are therefore set based on [4] as $F_{max} = 140$ N and $k = 75$ N/mm. The moving masses of the UR and Kuka robot are 29 kg and 20 kg respectively. The effective robot mass m_R is therefore $M/2 + m_L$, a function of the total mass of the moving parts of the robot M and the effective payload m_L , which is zero in our case. These values together with the Eq. 1 mean that the permissible velocity is up to 122 mm/s for the UR robot and 160 mm/s for the Kuka robot in case of clamping. If there is no clamping, the permissible force is doubled to 280 N and thus also the velocities are higher, namely 260 mm/s for the UR and 320 mm/s. The difference is due to the weight difference between the robots.

F. 2D Collision-Force-Map

The CFM proposed by [19] uses a linear model derived from the data to predict the impact force. The model is a second degree polynomial of the form:

$$\log(F) = \beta_0 + \beta_1 \cdot v + \beta_2 \cdot d + \beta_3 \cdot d^2 \quad (2)$$

The parameters are robot-, software-, and application-specific and are suggested to be determined by performing a large number of measurements (see Section II-A).

G. 3D Collision-Force-Map

The robot configuration influences the forces exerted upon impact. However, analytically calculating the exact forces is complicated as they are the result of not only the reflected mass of the system but also the torques of the robot joints and the often proprietary reaction behaviors of the robot (see for example [16], [18]).

We suggest to take into account also the height of the impact location in the linear equation Eq. 2. Also, this model can be instantiated for a given robot by a few training measurements and thus would allow a faster prototyping of a safe workplace. The model uses the actual impact forces of the given robot and does not rely merely on the single spring model from PFL. The resulting extension of Eq. 2 is:

$$\begin{aligned} \log(F) = & \beta_0 + \beta_1 \cdot v + \beta_2 \cdot d + \beta_3 \cdot d^2 + \\ & + \beta_4 \cdot v^2 + \beta_5 \cdot h + \beta_6 \cdot h^2 + \beta_7 \cdot d \cdot h^2 \end{aligned} \quad (3)$$

It is important to add the height parameter to the model, because as can be seen later in Fig. 8 and Fig. 9, the force distribution varies with the height from the robot base. We investigated the significance of the members of the linear model, but the form provided in Eq. 3 the best results. The additional members allow also for a better fit between the two tested robot arms.

III. RESULTS

In the following sections, we show the measured impact force values and derive the instances of the 3D CFM equation, Eq. 3, for each of the robots.

A. Quasi-static clamping and pressure

The UR robot shows only the Phase I from the force profile (see Section II-E and Fig. 4), a comparison with the Kuka robot can be seen in Fig. 6. This allows us to change the maximal permitted force of the UR robot to 280 N, as there is no direct clamping after the collision. This assumption changes the maximal expected permissible velocity for this robot computed in Section II-E from 122 mm/s to 260 mm/s. With the Kuka, both phases are present. However, our work focused on the initial peak impact. Notice that the Kuka robot showed a damped harmonic movement upon impact, as visible from Fig. 6, that was influenced by proprietary robot control behavior.

B. Measurements of peak impacts on UR

We collected measurements first on the UR robot to verify the results from [19] on a setup with only slight differences (e.g., the Airskin on our robot). We measured the impact forces on the given grid of positions, resulting in a total number of 444 measurements—119 for verification of the CFM and 325 for the 3D CFM. The collected data had a mean standard deviation of 1.12 N and maximal standard deviation of 3.85 N, which demonstrates high repeatability of the impacts.

At first, we wanted to prove the assumption of identical force over concentric circles from [19]. For that purpose, we used the 119 measurements on concentric circles in various positions and heights. Over these measurements, the maximal error with respect to the prediction of CFM was 10 N (3.5 %) and a mean error of 1 N (0.05 %). Considering the certified error of measuring device, which is up to 3 N, these values confirm the assumption of concentric circles around the base of the robot.

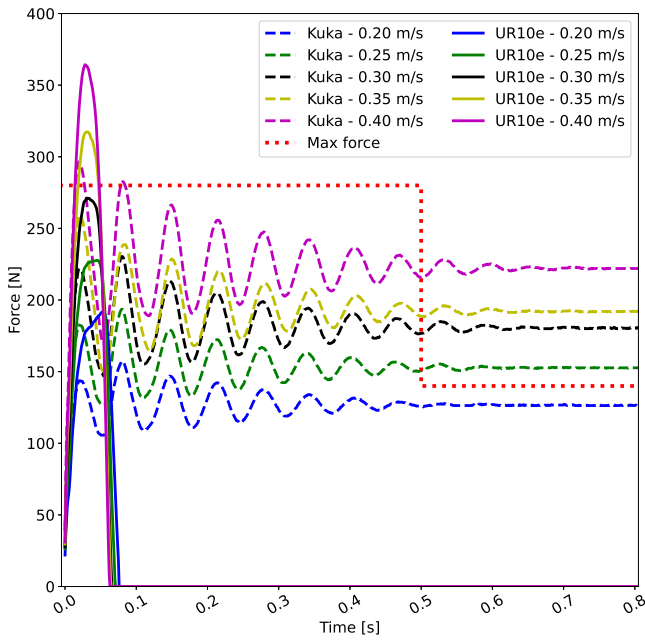


Fig. 6: Force in time graphs comparison for both robots and 5 different velocities.

		max UE [% / N]	mean UE [% / N]	max OE [% / N]	mean OE [% / N]
UR10e	Ts	5.57 / 20.06	1.87 / 5.60	9.46 / 37.40	3.15 / 9.47
	All	6.96 / 21.52	-	9.46 / 37.40	-
Kuka 30 Nm	Ts	9.57 / 22.96	2.64 / 7.29	8.66 / 15.24	3.13 / 8.32
	All	9.57 / 22.96	-	8.66 / 15.24	-
Kuka 10 Nm	Ts	5.58 / 18.75	2.04 / 5.32	5.39 / 15.79	1.77 / 4.64
	All	5.58 / 18.75	-	5.94 / 21.49	-

TABLE I: Table of relative errors for all robots and settings. **UE** stands for underestimation and **OE** for overestimation. **Ts** stands for test set and **All** for whole dataset.

Finally as mentioned in Section II-A, we fit the model with as little data as possible—this leads to a division of our 325 measurements into two parts. While taking only the odd-numbered positions, heights and steps we get 76 measurements to be used as training data and 249 measurements for testing the model performance. The resulting model is: $\log(F) = 6.3499 - 2.1829 \cdot d + 0.0854 \cdot d^2 + 5.4993 \cdot v - 4.1796 \cdot v^2 - 1.1552 \cdot h - 5.1532 \cdot h^2 + 6.4459 \cdot d \cdot h^2$. Figure 7 shows the 4D continuous representation of sampled robot’s workspace, showing relations between all variables.

As can be seen in Table I, the maximal underestimation over the testing set (249 measurements in the remaining positions, heights and speeds) is 5.57 % (20.06 N) and the mean underestimation is 1.87 % (5.60 N). Overestimation is slightly higher, 9.46 % (37.40 N) at maximum and 3.15 % (9.47 N) on average. The error over the whole 3D CFM dataset is underestimating slightly more, 6.96 % (21.52 N). But the low underestimation permits the use of this method to design a safe application. The higher overestimation is probably caused by the lack of accurate force values for high-valued impacts because we discarded the unreliable values above 500 N.

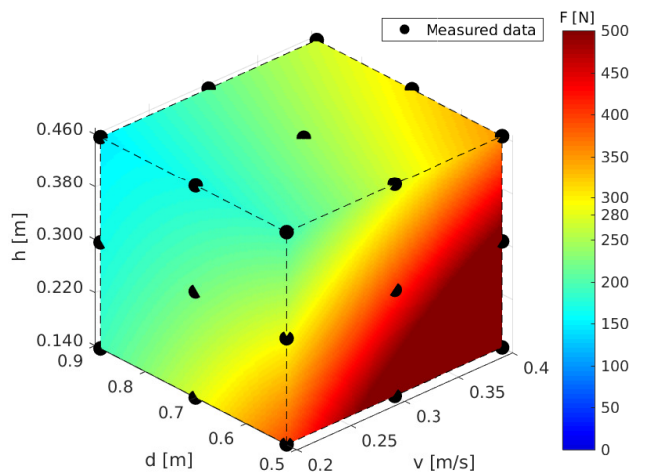


Fig. 7: 4D representation of sampled workspace for UR10e robot. Colour represents the force to enable 4D representation. Black points are showing measured training data capturing the measurement grid from Fig. 2.

C. Measurements of peak impacts on Kuka

As stated earlier, we collected values with two different safety settings, restricted to 10 and 30 Nm of external torque at any joint.

The dataset with 30 Nm of external torque is composed of 372 measurements divided by the same method as previously into two sets: 79 training and 293 testing ones. The model for this robot and settings is given by the equation: $\log(F) = 7.0230 - 5.3825 \cdot d + 2.2193 \cdot d^2 + 6.4174 \cdot v - 5.2391 \cdot v^2 - 0.4177 \cdot h - 5.4061 \cdot h^2 + 6.1983 \cdot d \cdot h^2$.

In this case, the maximal underestimation error is 9.57 % (22.96 N) with a mean underestimation of 2.64 % (7.29 N). The overestimation is comparable to UR robot, with a mean value of 3.13 % (8.32 N) and with the maximal error of 8.66 % (15.24 N). In Table I, we can see that underestimation is worse than in case of UR robot. Following Section II-A, these errors would be used to determine the necessary margin for a conservative safe model of the robot.

The dataset was collected with a mean standard deviation of 0.58 N and with a maximum of 3.09 N. As the repeatability seems to be very high, we decided to measure the forces in next experiment only with one repetition. The resulting dataset contains 125 measurements with restriction to 10 Nm of external torque with 27 training and 98 testing measurements.

The resulting model for Kuka with 10 Nm is the equation $\log(F) = 6.7037 - 5.2110 \cdot d + 2.2633 \cdot d^2 + 6.5781 \cdot v - 5.0646 \cdot v^2 - 0.1676 \cdot h - 5.2812 \cdot h^2 + 5.7739 \cdot d \cdot h^2$. How closely the model corresponds to the measured data is illustrated in Figure 9. The maximal underestimation is comparable to UR robot with 5.58 % (18.75 N) and an average of 2.04 % (5.32 N). The overestimation is even lower than with the previous safety settings with a peak value of 5.39 % (15.79 N) and 1.77 % (4.64 N) on average. These errors, together with the

change in model in comparison to the Kuka with 30 Nm of external torque, show that safety settings are an important factor in the impact force modelling.

IV. DISCUSSION AND CONCLUSION

The data presented in results do not fit exactly our model. However, the question is if our model is able to predict the impact force better than the two other simple models for the task. The following sections present a comparison with the PFL and CFM model predictions.

A. Comparison of PFL suggested values to our results

The PFL formulae suggest only one velocity limit for the whole robot workspace if the robot weight is the same. This means a one-to-one correspondence between velocity and impact force for a fixed weight. However, one velocity can lead to various impact forces, see Fig. 8 and 9. Besides, the actual impact forces can be below but also above the impact force predicted by PFL.

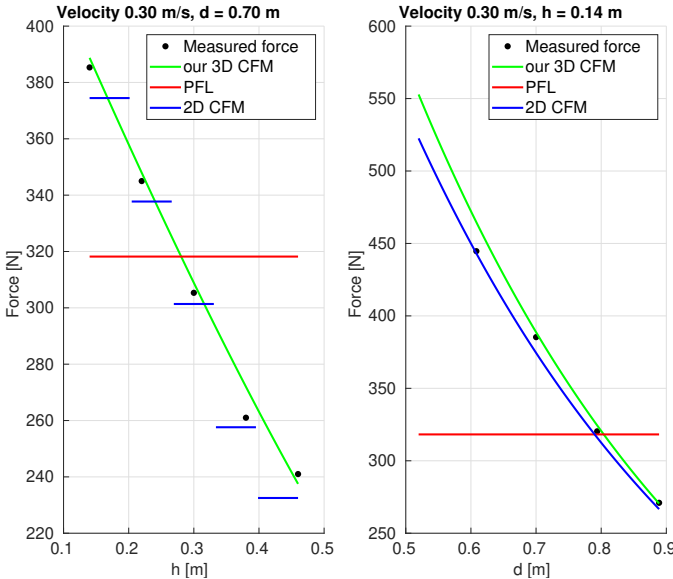


Fig. 8: UR10e impact force model comparison of the Power and Force Limiting model, the original 2D Collision Force Map and our 3D Collision Force Map.

B. Comparison with the 2D Collision-Force-Map

We used the least-squares method to fit our data to the CFM model (Eq. 2) using the lowest, middle and largest velocity and d . Since there is no height parameter in this model, it is necessary to create an individual model for each height level to obtain more precise results. For an example comparison see Fig. 8 and 9. As can be seen in Table II, the CFM over-estimates less. On the other hand, it underestimates significantly more than our 3D CFM model. Also, our formula has lower errors on the Kuka robot and this suggests it generalizes better.

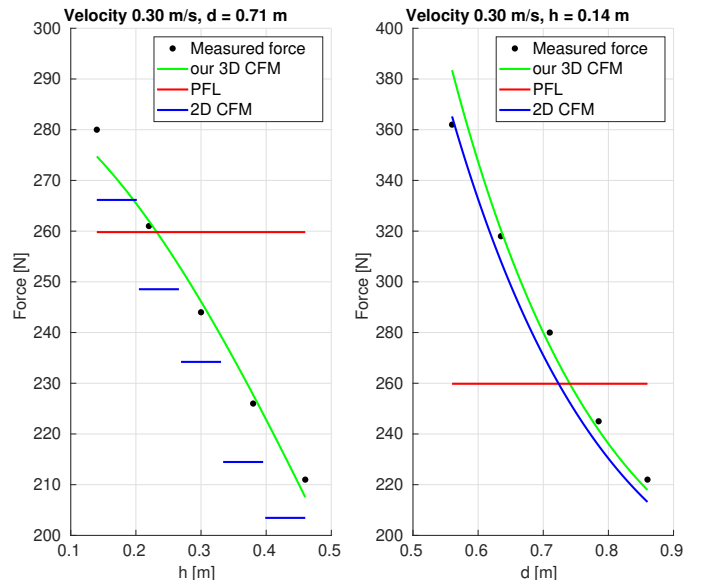


Fig. 9: Kuka with 10 Nm torque limit impact force model comparison of the Power and Force Limiting model, the original 2D Collision Force Map and our 3D Collision Force Map.

		max UE [% / N]	mean UE [% / N]	max OE [% / N]	mean OE [% / N]
UR10e	Ts	6.51 / 14.60	2.23 / 6.33	7.56 / 11.22	1.76 / 5.17
	All	6.51 / 14.60	-	9.13 / 13.21	-
Kuka 30 Nm	Ts	12.01 / 28.83	3.94 / 10.91	7.32 / 27.67	2.73 / 7.19
	All	12.01 / 28.83	-	7.89 / 22.14	-
Kuka 10 Nm	Ts	8.70 / 29.23	3.04 / 7.59	5.24 / 21.76	2.18 / 5.82
	All	8.70 / 29.23	-	5.24 / 21.76	-

TABLE II: Table of relative errors for all robots and settings based on models for every height. **UE** stands for underestimation, and **OE** for overestimation. **Ts** stands for test set and **All** for whole dataset. Gray values are worse compared to our model.

C. Conclusion and future work

We presented measurements of impact forces on two collaborative robots and suggested an impact force distribution model that can serve as a basic tool for the design of a human-robot collaborative workspace. Our model describes the initial peak impact force of clamping contact scenarios more precisely than the PFL [4] or CFM models [19] by taking into account the impact location's distance and also its height with respect to the robot base.

Nevertheless, the Power and Force Limiting collaboration regime admits multiple extensions. For the evaluation of a contact scenario, also the pressure values should be taken into account as they reflect better the properties of the impactor's surface. We did not take this aspect into account in our current study. It allows also purely transient contacts, i.e. no clamping, that allow higher velocities. These should be covered in future work where the proper movement of the impacted object should be modelled. Similarly, the regime permits the risk reduction by the application of various passive measures, their effect would be evaluated also in future studies.

REFERENCES

- [1] “ISO 8373 Robots and robotic devices – Vocabulary,” International Organization for Standardization, Geneva, CH, Tech. Rep., 2012.
- [2] F. Vicentini, “Terminology in safety of collaborative robotics,” *Robotics and Computer-Integrated Manufacturing*, vol. 63, p. 101921, 2020.
- [3] “ISO 10218 Robots and robotic devices – Safety requirements for industrial robots,” International Organization for Standardization, Geneva, CH, Tech. Rep., 2011.
- [4] “ISO/TS 15066 Robots and robotic devices – Collaborative robots,” International Organization for Standardization, Geneva, CH, Tech. Rep., 2016.
- [5] F. Vicentini, “Collaborative robotics: a survey,” *Journal of Mechanical Design*, pp. 1–29, 2020.
- [6] N. Mansfeld, M. Hamad, M. Becker, A. G. Marin, and S. Haddadin, “Safety Map: A Unified Representation for Biomechanics Impact Data and Robot Instantaneous Dynamic Properties,” *IEEE Robotics and Automation Letters*, vol. 3, no. 3, pp. 1880–1887, 2018.
- [7] N. Lucci, B. Lacevic, A. M. Zanchettin, and P. Rocco, “Combining Speed and Separation Monitoring with Power and Force Limiting for Safe Collaborative Robotics Applications,” *IEEE Robotics and Automation Letters*, 2020.
- [8] P. Sváry, M. Tesar, J. K. Behrens, and M. Hoffmann, “Safe physical HRI: Toward a unified treatment of speed and separation monitoring together with power and force limiting,” in *2019 IEEE/RSJ International Conference on Intelligent Robots and Systems (IROS)*, 2019, pp. 7580–7587.
- [9] H. Shin, K. Seo, and S. Rhim, “Allowable maximum safe velocity control based on human-robot distance for collaborative robot,” in *2018 15th International Conference on Ubiquitous Robots (UR)*. IEEE, 2018, pp. 401–405.
- [10] F. Ferraguti, M. Bertuletti, C. T. Landi, M. Bonfe, C. Fantuzzi, and C. Secchi, “A control barrier function approach for maximizing performance while fulfilling to ISO/TS 15066 regulations,” *IEEE Robotics and Automation Letters*, 2020.
- [11] P. Aivaliotis, S. Aivaliotis, C. Gkournelos, K. Kokkalis, G. Michalos, and S. Makris, “Power and force limiting on industrial robots for human-robot collaboration,” *Robotics and Computer-Integrated Manufacturing*, vol. 59, pp. 346–360, 2019.
- [12] K. Suita, Y. Yamada, N. Tsuchida, K. Imai, H. Ikeda, and N. Sugimoto, “A failure-to-safety “Kyozon” system with simple contact detection and stop capabilities for safe human-autonomous robot coexistence,” in *Proceedings of 1995 IEEE International Conference on Robotics and Automation*, vol. 3. IEEE, 1995, pp. 3089–3096.
- [13] M. Y. Park, D. Han, J. H. Lim, M. K. Shin, Y. R. Han, D. H. Kim, S. Rhim, and K. S. Kim, “Assessment of pressure pain thresholds in collisions with collaborative robots,” *PloS one*, vol. 14, no. 5, 2019.
- [14] D. Han, M. Y. Park, H. Shin, K. S. Kim, and S. Rhim, “Identifying Safety Conditions of Human-Robot Collision based on Skin Injury Analysis,” in *2018 15th International Conference on Ubiquitous Robots (UR)*. IEEE, 2018, pp. 420–423.
- [15] S. Haddadin, “Physical safety in robotics,” in *Formal modeling and verification of cyber-physical systems*. Springer, 2015, pp. 249–271.
- [16] S. Haddadin, A. De Luca, and A. Albu-Schäffer, “Robot collisions: A survey on detection, isolation, and identification,” *IEEE Transactions on Robotics*, vol. 33, no. 6, pp. 1292–1312, 2017.
- [17] N. Kovincic, H. Gattringer, A. Müller, M. Weyrer, A. Schlotzhauer, L. Kaiser, and M. Brandstötter, “A model-based strategy for safety assessment of a robot arm interacting with humans,” *PAMM*, vol. 19, no. 1, p. e201900247, 2019.
- [18] N. Kovincic, H. Gattringer, M. Andreas, and M. Brandstötter, “A Boosted Decision Tree Approach for a Safe Human-Robot Collaboration in Quasi-static Impact Situations,” *Advances in Service and Industrial Robotics: Results of RAAD*, p. 235, 2020.
- [19] A. Schlotzhauer, L. Kaiser, J. Wachter, M. Brandstötter, and M. Hofbaur, “On the trustability of the safety measures of collaborative robots: 2D Collision-force-map of a sensitive manipulator for safe HRC,” in *2019 IEEE 15th international conference on automation science and engineering (CASE)*. IEEE, 2019, pp. 1676–1683.
- [20] D. Mewes and F. Mauser, “Safeguarding crushing points by limitation of forces,” *International journal of occupational safety and ergonomics*, vol. 9, no. 2, pp. 177–191, 2003.
- [21] “ISO 12100 Safety of machinery – General principles for design – Risk assessment and risk reduction,” International Organization for Standardization, Geneva, CH, Tech. Rep., 2010.